

Article

Geological and 3D Image Analysis toward Protecting a Geosite: The Case Study of Falakra, Limnos, Greece

Ioannis K. Koukouvelas ^{1,*}, Aggeliki Kyriou ¹, Konstantinos G. Nikolakopoulos ¹, Georgios Dimaris ², Ioannis Pantelidis ¹ and Harilaos Tsikos ¹

¹ Department of Geology, University of Patras, 265 04 Patras, Greece; knikolakop@upatras.gr (K.G.N.); geo14136@ac.upatras.gr (I.P.); htsikos@upatras.gr (H.T.)

² George Dimaris Technical Office, Mirina, 81400 Limnos, Greece; george.dimaris@gmail.com (G.D.)

* Correspondence: iannis@upatras.gr

Abstract: The Falakra geosite is located at the northern shoreline of the island of Limnos, Greece, and exhibits an array of unusual geomorphological features developed in late Cenozoic sandstones. Deposition of the primary clastic sediments was overprinted by later, low-temperature hydrothermal fluid flow and interstitial secondary calcite formation associated with nearby volcanic activity. Associated sandstone cannonballs take center stage in a landscape built by joints, Liesegang rings and iron (hydr)oxide precipitates, constituting an intriguing site of high aesthetic value. The Falakra geosite is situated in an area with dynamic erosion processes occurring under humid weather conditions. These have evidently sculpted and shaped the sandstone landscape through a complex interaction of wave- and wind-induced erosional processes aided by salt spray wetting. This type of geosite captivates scientists and nature enthusiasts due to its unique geological and landscape features, making its sustainable conservation a significant concern and topic of debate. Here, we provide detailed geological and remote sensing mapping of the area to improve the understanding of geological processes and their overall impact. Given the significance of the Falakra geosite as a unique tourist destination, we emphasize the importance of developing it under sustainable management. We propose the segmentation of the geosite into four sectors based on the corresponding geological features observed on site. Sector A, located to the west, is occupied by a lander-like landscape; to the southeast, sector B contains clusters of cannonballs and concretions; sector C is characterized by intense jointing and complex iron (hydr)oxide precipitation patterns, dominated by Liesegang rings, while sector D displays cannonball or concretion casts. Finally, we propose a network of routes and platforms to highlight the geological heritage of the site while reducing the impact of direct human interaction with the outcrops. For constructing the routes and platforms, we propose the use of serrated steel grating.

Keywords: Falakra geosite; geological heritage; UAV; TLS; mapping; sustainability; Limnos; Greece

Academic Editor:

Amin Beiranvand Pour

Received: 27 December 2024

Revised: 24 January 2025

Accepted: 30 January 2025

Published: 31 January 2025

Citation: Koukouvelas, I.K.; Kyriou, A.; Nikolakopoulos, K.G.; Dimaris, G.; Pantelidis, I.; Tsikos, H. Geological and 3D Image Analysis toward Protecting a Geosite: The Case Study of Falakra, Limnos, Greece. *Minerals* **2025**, *15*, 148. <https://doi.org/10.3390/min15020148>

Copyright: © 2025 by the authors. Licensee MDPI, Basel, Switzerland. This article is an open access article distributed under the terms and conditions of the Creative Commons Attribution (CC BY) license (<https://creativecommons.org/licenses/by/4.0/>).

1. Introduction

With the beginning of the 21st century, the promotion, safeguarding, and sustainable management of geological heritage sites are becoming increasingly important to governments, local communities, and individuals. Geological heritage is important because it represents key sites for understanding the processes that contribute to the evolution of the Earth. Travel and tourism in Greece are strong components of the country's gross domestic product and boost employment. At present, both economic sectors are recording a strong recovery (+104% in 2023) compared to pre-pandemic levels (2019) [1]. Arrivals in 2024 show an additional 7% increase over the records for the previous year [2]. The preferred destination for a significant part of this tourism is the NE Aegean islands, famous for their rich culture and history. Limnos, an island in the NE Aegean Sea, is one of those

islands, characterized by an impressively diverse landscape, which is home to many archaeological sites, fortresses, and traditional villages [3].

Greece and the surrounding Aegean and Ionian Sea islands were formed during complex geological processes occurring at the margins of three convergent lithospheric plates [4]. This complexity has endowed the country with more than three hundred geosites, some of which have been formally designated as part of the eight UNESCO geoparks around the country [5].

Following the recent recovery in tourist influx, the management structures of natural resources, such as geosites, must navigate the added pressure that increasing tourism brings with it. Geosites are defined as geomorphological and geological features (ranging from small, isolated structures to significant outcrops) that provide scientific, educational, and cultural information about the processes that contribute to the evolution of the Earth [6]. To this end, the sustainable conservation of a high aesthetic geosite is a matter that deserves mature and critical assessment because it attracts both scientists and nature enthusiasts. This applies especially to those sites that are most vulnerable to degradation by anthropogenic and/or natural factors [7].

This work is a multidisciplinary analysis of the Falakra geosite of Limnos. It utilizes basic geological, meteorological, and remote sensing techniques to enhance understanding of the formation and vulnerability of this geosite from an Earth science perspective. The data collected provide a strong basis that facilitates the protection and sustainable management of the highly aesthetic Falakra geosite. Our techniques include traditional mapping of the site and its geological structures, describing erosion processes and their effects, and conducting basic mineralogical and geochemical characterization of the rocks to provide insights into their origin and fluid interaction history. Emphasis is placed in elucidating the complex interplay of background geology with present-day active erosional processes in shaping the rocks and informing present and future conservation strategies for the geosite. Remote sensing analysis through terrestrial LiDAR and UAV flights allows for the optimal delineation of routes and visitor navigation through the site, as well as the establishment of a monitoring network.

2. Materials and Methods

The Falakra locality is a well-known geosite located in the northern part of Limnos. The geosite is renowned for its unusual and aesthetically impressive geological formations both in a local and international context. Prior to our first field visit in November 2022, we had noted the lack of a comprehensive locality map showing the geosite boundaries, existing access routes, key geological features, and other points of potential interest (e.g., visitor kiosks and/or similar structures). In addition, little is available in the relevant literature about the processes that led to the formation of various geological features at the geosite on all spatial scales. Recognizing the importance of the Falakra geosite, we employed non-catastrophic sampling to collect 16 representative sandstone samples capturing key geological features of potential significance to formation modelling and interpretation (e.g., joints, iron (hydr)oxide rings/impregnations, calcite vein infills, etc). The samples were derived from dismembered portions of the outcrops, such as fragmented cannonballs and jointed sandstones, variously enriched/filled with iron (hydr)oxides and/or calcite. Two clay-rich horizons intercalated among the sandstones were also included in our sampling.

Alongside the sampling campaign, we conducted a precise mapping of the geological features and analyzed the processes behind the natural evolution of the Falakra geosite, by applying traditional geological mapping and remote sensing techniques (Figure 1). These include outcrop description and analysis, stratigraphy, and structural analysis of the study area, supported further by remote sensing techniques such as laser scanning survey and UAV (Unmanned Aerial Vehicle) photogrammetry. A flowchart of the applied methodology is depicted in Figure 1.

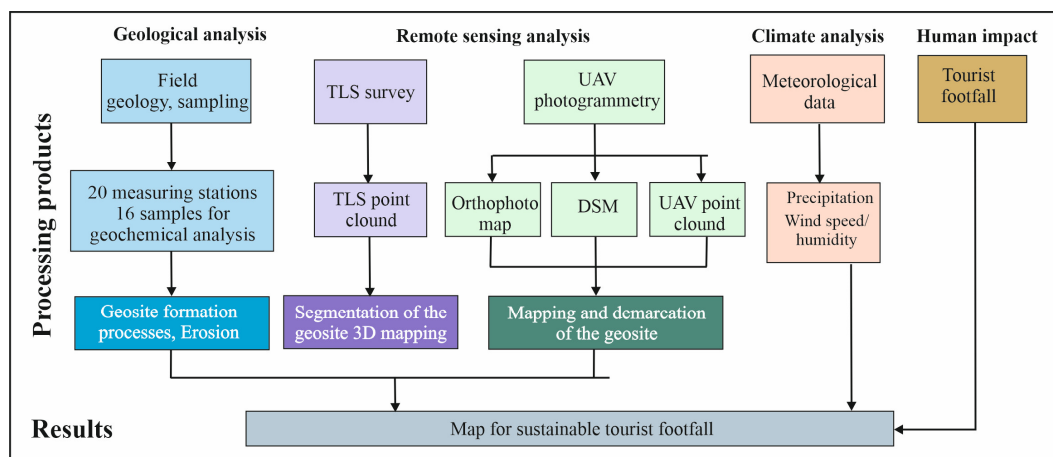


Figure 1. Flowchart of the applied methodology.

For the laser scanning survey, a Leica BLK360 was utilized (Figure 2a). The sensor is equipped with Visual Inertial System (VIS) technology that combines multi-positioned scans via the Visual Simultaneous Localization and Mapping (SLAM) technique [8]. Specifically, the SLAM algorithm computes the 3D coordinates of specific features from two or more observation locations and uses these coordinates to define the upcoming position. The collected data were processed in Leica Cyclone 360 and 3DR software. The laser scanning at the geosite was validated by UAV observations. A DJI Matrice 300 was utilized to execute the UAV mapping (Figure 2b). Such a quadcopter is equipped with a Zenmuse ZH20 (4.5 mm) camera, capturing 290 images of 4056 × 3040 pixels using a mechanical shutter to minimize lens distortions (Figure 2b). The flight was performed at 80 m altitude. To process the UAV images, we used Agisoft Metashape software (v. 2.0.1., Agisoft LLC, St. Petersburg, Russia) and Structure-from-Motion photogrammetry (SfM) [9–11]. Detailed information on image processing has been extensively reported in previous studies [12,13]. The processing products, i.e., an orthophoto, a Digital Surface Model (DSM), and a point cloud covering the area of interest are projected onto the Hellenic Geodetic Reference System 1987. Moreover, we analyzed meteorological parameters such as precipitation, temperature, humidity, wind speed, and wind direction to examine their influence on the erosion of the geosite.



Figure 2. (a) Laser scanning survey using a Leica BLK360; (b) an indicative photo of the DJI Matrice 300 with a Zenmuse ZH20 camera on board.

Seven samples of sandstone were analyzed for basic mineralogical and bulk geochemical characterization. Additionally, two mineralogically end-member samples were also included in the analyses, namely one of fine-veined calcite crosscutting one of the sandstone samples, and another from a dm-thick clay-rich horizon within the sandstone succession. All samples were fragmented and rinsed thoroughly with deionized water to eliminate superficial salt deposits from seawater spray as much as possible. The samples were then pulverized into fine powder and analyzed for bulk mineralogy using XRD instrumentation at the University of Patras, followed by bulk geochemical analyses on fused

beads produced from the same sample powders, using combined XRF and ICP-MS instrumentation at Stellenbosch University, South Africa. Complete data tables can be found in the supplementary file.

3. Geological Setting and Meteorological Parameters of the Study Area

3.1. Geological Setting of the Study Area

Limnos Island is situated in the southern part of the so-called Thrace Basin [14–19]. The basin covers an area of about 20,000 km², from mainland Greece and Turkey in the north, the Biga Peninsula in the east, and the North Aegean Islands in the south. The basin accommodated a series of shallow- to deep-marine turbidite deposits ranging in age from Upper Eocene to Lower Oligocene [20] and Miocene volcanic rocks [21,22] (Figure 3). The Falakra geosite belongs to or was formed within these marine turbidite deposits. The sediments were deposited in deltas advancing into freshwater, but near coastal environments [20].

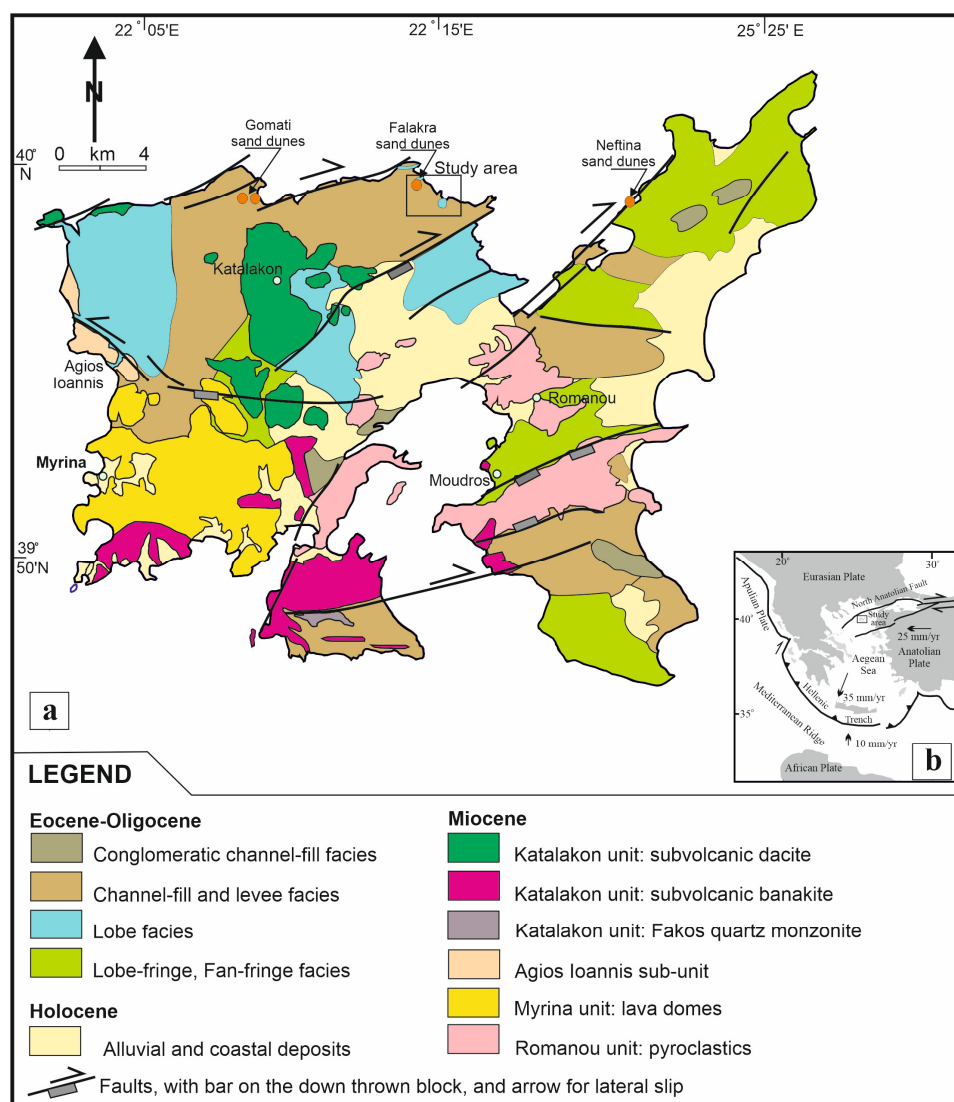


Figure 3. (a) Geological structure of the island of Limnos [22,23], also showing the study area and sand dune locations across the north coast of Limnos. (b) Inset shows the allocation of Limnos Island in Greece.

The sedimentary history of Limnos is complex and includes Upper Eocene outer and inner fan deposits that change to coarser sediments across the Eocene–Oligocene boundary [20]. During the Lower Oligocene (~31 Ma), the prevailing sediments become slope-

to-shelf facies deposits [20]. The miocene volcanic rocks of Limnos constitute three successions belonging to an early stratovolcano, of which only remnants remain [22,23]. The older succession of the so-called Romanou Unit (22.3 ± 0.7 Ma) consists of pyroclastic and volcanoclastic rocks in the eastern half of the island. The second unit, the Katalakon Unit (21.3–20.2 Ma), includes subvolcanic stocks, dykes, and a ~20 Ma quartz–monzonite body in the Fakos area. The Katalakon Unit also intrudes the flysch basement in the western half of the island (Figure 3). The younger volcanic succession, the Myrina Unit (17.9–19.3 Ma), occupies a NW-trending graben bounded on its northern side by the sinistral Kaspakas–Kontias fault [23,24]. It consists of domes and flows in the southwestern part of the island. A major E-W fault system in the southern part of the island is the most important control on magmatism. It locates the primitive banakite rocks of the Katalakon Unit, dykes and domes within the Romanou pyroclastic succession, and the late domes of the Myrina Unit [22]. The island of Limnos is also dissected by a series of active faults that are considered genetically related to the North Anatolian Fault and its propagation in the North Aegean Sea [23–25] (Figure 3). The Falakra geosite is located on the north coast of Limnos, where channel-fill and levee facies deposits are exposed [20]. The previously mentioned volcanic rocks of the Katalakon Unit are in close geologic proximity to the Falakra geosite, making the study of possible sedimentary and volcanic processes acting in the same area over the Tertiary challenging [22,23].

3.2. Meteorological Parameters at Falakra Geosite

In our efforts to evaluate the factors affecting the sustainability of the Falakra geosite, we analyzed meteorological parameters such as precipitation, temperature, humidity, wind speed, and wind direction. The lowest monthly precipitation is recorded in August, at 6.3 mm, compared to a maximum of 84.7 mm for December (Figure 4a). The annual average precipitation is 502.7 mm for the period 1974 to 2010, with 46 % of the precipitation volume corresponding to the winter months for the Limnos meteorological station [26]. In addition, the prevailing wind direction is from NE, and the monthly mean wind power ranges from 6.9 to 11.2 knots.

For the evaluation of meteorological parameters at Falakra geosite, we utilized ERA5-Land, which constitutes a re-analysis dataset that provides systematic and consistent observations of land variables over several decades at an improved spatial resolution (Figure 4b). The product contains 50 variables resulting from the combination of model data with daily in situ and space-borne observations. Such an approach provides important information about climate evolution over time. The dataset was produced by the Copernicus Climate Change Service (C3S), which was implemented by the European Centre for Medium-Range Weather Forecasts (ECMWF) on behalf of the European Commission. For 2023, the monthly precipitation on the geosite in August is estimated at 1 mm, compared to 109 mm in December. The annual average precipitation is 36 mm with 70–80% of the volume corresponding to the winter months. In addition, the prevailing wind direction is east–northeast, at speeds of up to 50km/h (Figure 4c). Such a direction strongly affects the Falakra geosite, which faces northeast (Figures 3 and 5a).

Overall, the data presented above indicate that the Falakra geosite is located in an area with mild climatic conditions from May until October, with maximum temperatures rarely exceeding 30° C, with relatively high humidity, and common winds from NE.

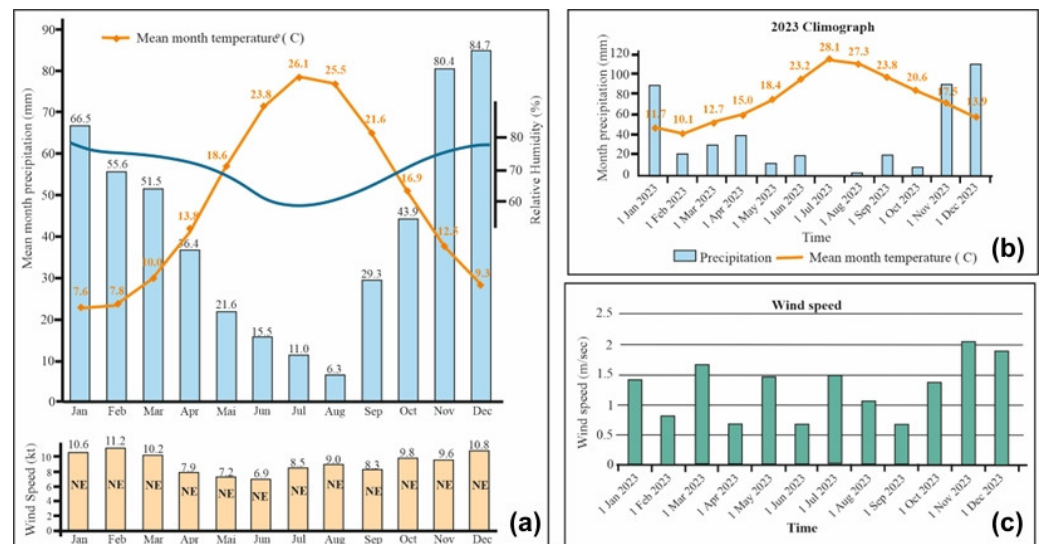


Figure 4. (a) Long-term meteorological data derived from the Limnos meteorological station. (b) Climograph displaying the average monthly temperature and precipitation for 2023, as derived from ERA5-Land. (c) Diagram showing the wind speed per month for 2023, as derived from ERA5-Land.

4. Falakra: A Geosite Under Touristic Stress

The Falakra geosite has long been considered an important landscape in Limnos, with the visiting period extending for up to six months every year, i.e., during the summer and autumn (Figure 5). Local tradition holds that the Falakra geosite reminisces hairless human scalps, a name given from the naturally occurring round to sub-round concretions of sedimentary rock. These concretions formed during geological processes from the Tertiary to the present. The concretions, in current scientific terminology, are classified as 'cannonball rocks' and are hereinafter referred to simply as cannonballs for convenience. Cannonballs are fascinating formations with high aesthetic and touristic appeal that have captured the imagination of scientists and nature enthusiasts alike (Figures 5 and 6) [27]. The term "cannonball" originates from the Cannon Ball River in North Dakota, USA, where similar geomorphological features are widespread. Apart from the cannonballs, the Falakra geosite sandstones contain widespread evidence of Liesegang-style rings or bands [28] and joints filled with iron oxide and calcite precipitates. In particular, the Liesegang bands are recognized as successive thin layers at mm- to cm-scale that cut across the sandstone bedding. This is consistent with most localities worldwide, where typical rocks for the occurrence of Liesegang are indeed sandstones.

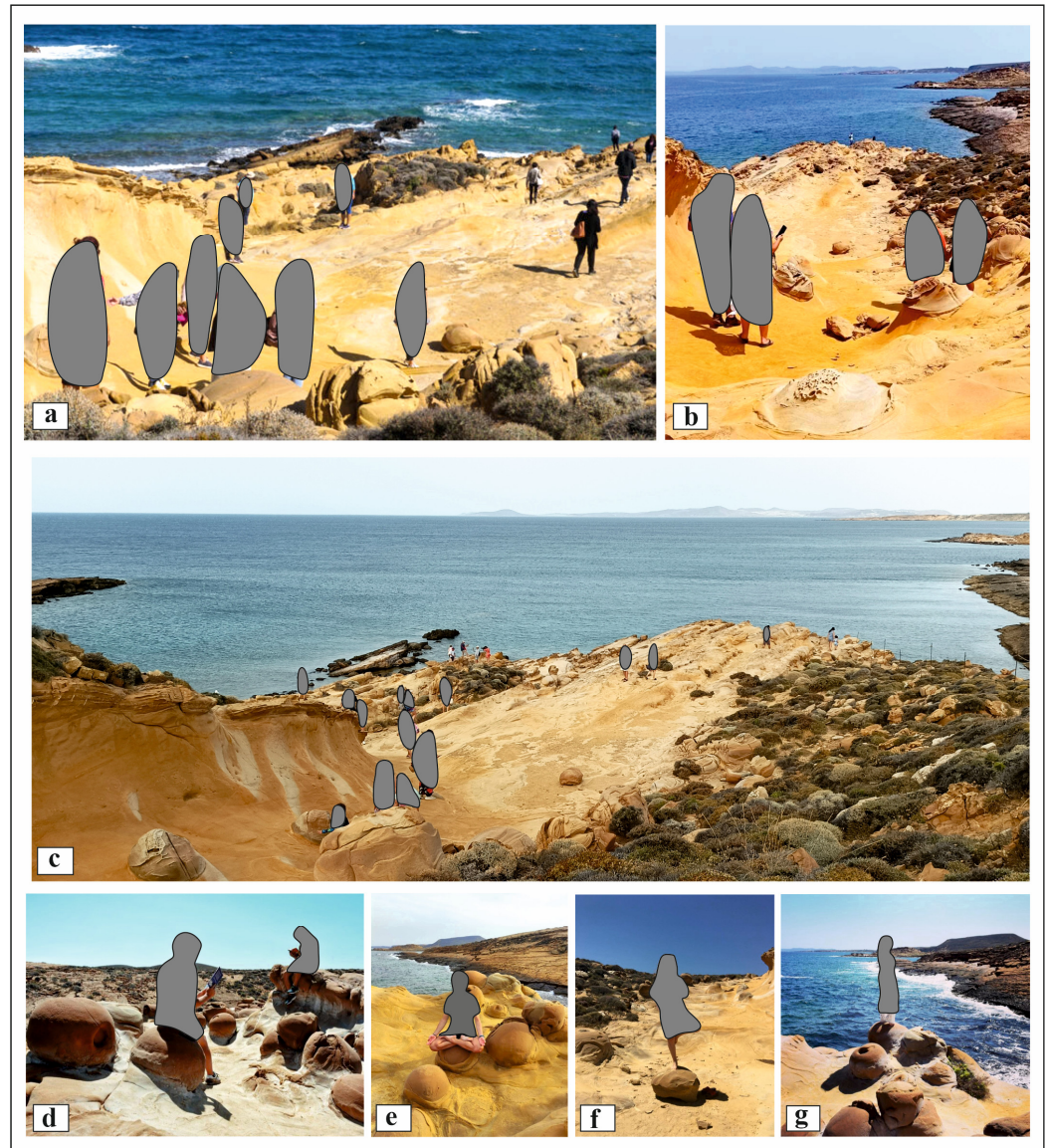


Figure 5. (a–c) Representative photographs displaying free access for tourists when visiting the geosite. The three photographs were taken facing northeast. (d–g) Typical scenes of visitors reading books, doing yoga, or standing on cannonballs and concretions. Photographs (d) and (f) were taken facing northwest, and photographs (e) and (g) were taken facing northeast.

The scientific and aesthetic appeal of the Falakra geosite has resulted in considerable publicity, as evidenced from more than thirty (30) websites and numerous social media posts. The geosite is a top target for a large portion of the tourists that choose Limnos as a holiday destination. During our two field campaigns in November 2022 and July 2023, more than thirty visitors per day were noted on site. During their visits, tourists are free to walk on the geosite and, in some cases, to rest on cannonballs, where they read books or even carry out yoga routines (Figure 5d–g).

It follows that the sustainability of the Falakra geosite, purely because of its high tourist footfall, is a matter that deserves attention. This adds to another key threat to the geosite, which is natural erosion. This was readily evident through the optical analysis of field photos from as recently as 2019 and during 2022–2023. Evidence for erosional effects at the Falakra geosite is registered in the loose sand concentrations at various places in the geosite and/or as the displacement and removal of rock debris (Figure 6).

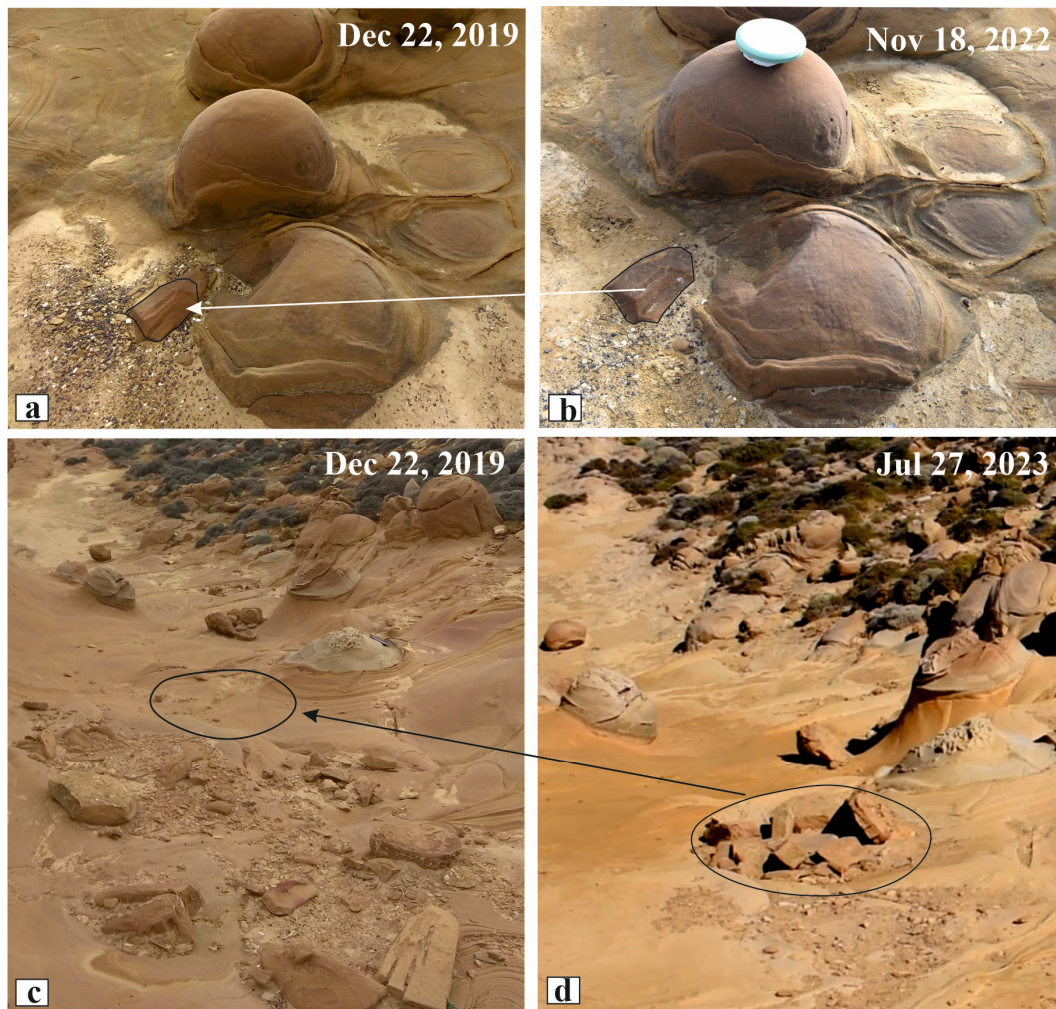


Figure 6. Representative rock outcrops showing progressive erosion in the Falakra geosite. (a,b) White arrows point to the areas accumulating sand concentration around cannonballs. The increase in erosion is observed as a progressive burial of a sandstone fragment, outlined with a black line, over an approximate period of three years. (c,d) Black arrows point to the downslope removal of sandstone fragments in the lander-like landscape.

5. Results

5.1. Mapping the Geosite Through 3D Vision Techniques

The processing of UAV and TLS data contributed to the creation of 3D models for the Falakra geosite. Figure 7 depicts the UAV orthophoto map, while TLS-based point cloud was used to facilitate the segmentation and definition of the prevalent geological features of the geosite. Specifically, the main entities of the geosite are the lander-like landscape, cannonballs, joints filled with iron (hydr)oxides, and cannonball casts. Liesengang rings are exposed across the entire geosite and are not confined to any particular sector. The produced models of the geological features are fully metric, and they can be used for various applications (management, protection, promotion, education etc.) by the local authorities or stakeholders.

In addition, we calculated the slope for the lander-like landscape. Figure 8 displays the result of the slope analysis. As observed, the lander-like landscape is defined by nine strides that exhibit a slope greater than 45%. This landscape occupies an area of approximately 141 m². The lowest stride is located at an elevation of 13.55 m and attains a height of 0.168 m. On the contrary, the highest stride is located at about 17.65 m and was measured at a height of 0.114 m. Generally, the height of the nine strides varies between 0.009 m to 0.522 m, while their width ranges from 0.910 m to 3.904 m. The lander-like landscape is the more sensitive in terms of erosion, since it is easily accessible to tourists as the main entrance to the geosite (see also Figure 6c and d).

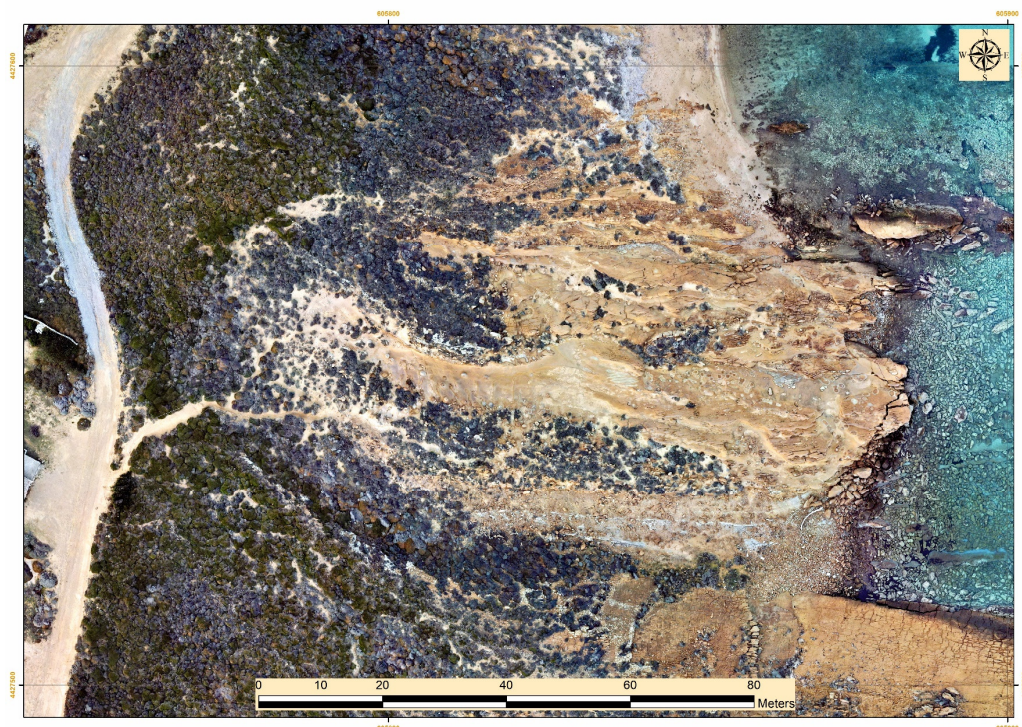


Figure 7. UAV orthophoto map of the Falakra geosite.

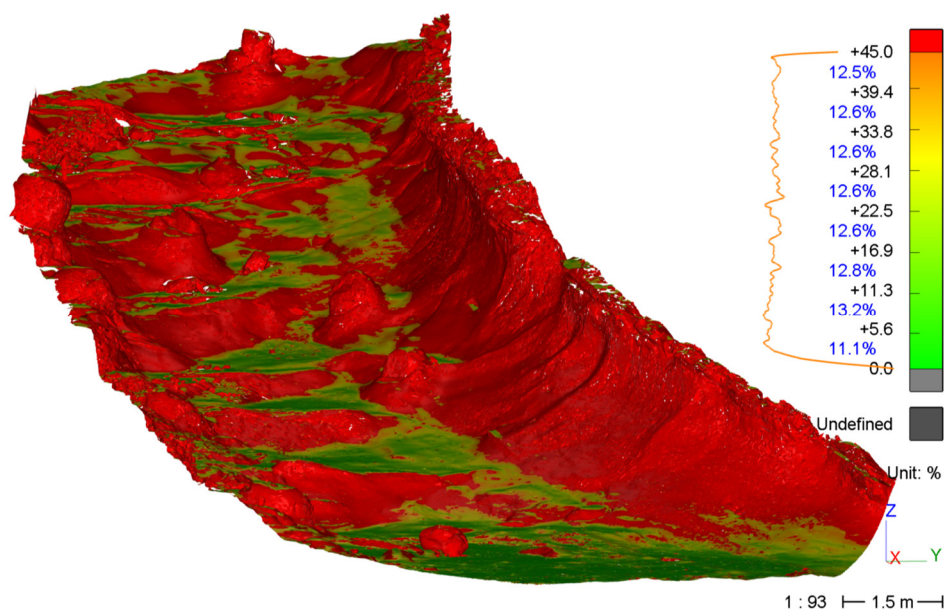


Figure 8. Slope analysis of the lander-like landscape, consisting of nine strides.

5.2. Geological and Geomorphological Mapping Results

Following the mapping of all key geological features at Falakra (cannonballs, jointed sandstones, Liesengang rings), we subdivided the geosite into four sectors based on the broad distribution patterns of the formations observed. Sector A includes the lander-like landscape at the westernmost end of the geosite (Figure 9). The lander-like landscape is defined by nine strides (Figure 9), each expressed by deep red Liesengang rings (Figure 9) or joints showing evidence of iron (hydr)oxide precipitation (inset in Figure 9b).

The lander-like formation measures 31.5 m in length and 6.5 m in width. In some cases, at the stride termination, there are rounded to sub-rounded cannonballs up to 1.7 m in diameter (Figure 9). Important for the aesthetic appeal of the lander-like landscape are the conspicuous Liesengang rings, forming a complex wavy and semi-concentric patterns that appear to mimic the movement of fluid fronts through permeable sandstone

(see blue bold letters a and b in Figure 9) are important for the aesthetic appeal of the lander-like landscape. The joint network that dissects the sandstones is thought to be integral part of the overall Liesengang system and is itself thought to have acted as added permeability network for fluid flow and iron (hydr)oxide precipitation (Figure 9b, inset). As the Liesengang rings and joints produce apparent erosion-resistant strips in the sandstone, we consider that the strides in the lander must be linked—at least partly—to the joints and the compositional characteristics of the sandstones. Whatever their exact origin, the Liesengang rings decorate the lander-like landscape of the geosite with captivating reddish hues in an otherwise monotonously yellowish sandstone (Figure 9b). During the mapping of this landscape, it was also noted that most of the cannonballs also exhibit honeycomb-style erosion (see inset in Figure 9a).

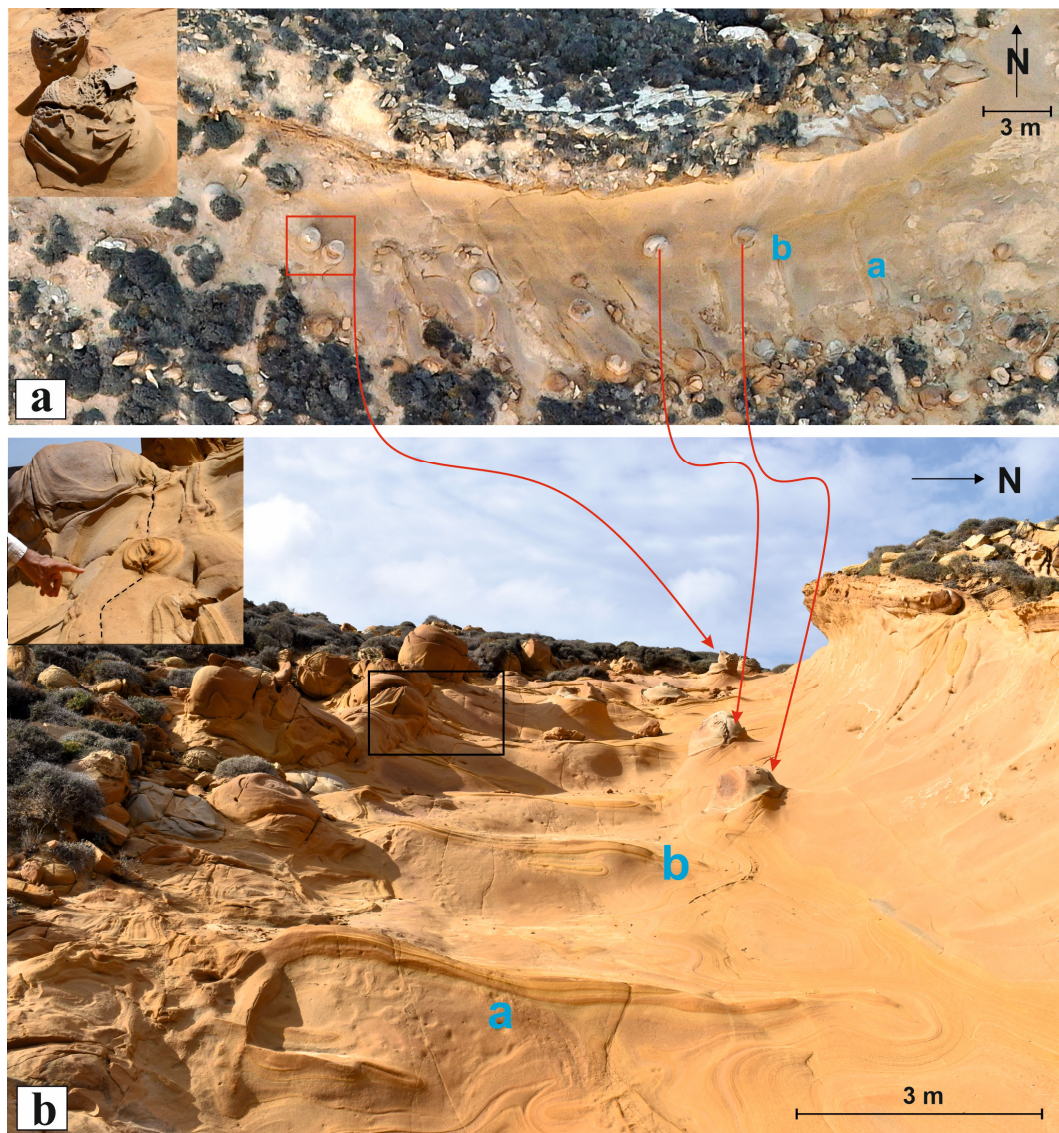


Figure 9. (a) The lander-like landscape from above. An image acquired by the UAV during the photogrammetric flight. See the nine strides forming the lander-like landscape. The inset shows two cannonballs with turtleback-structured honeycombs. For the location of the cannonball pair, see the red rectangle in the aerial view photo. (b) Field photo of the lander-like landscape showing the extensive presence of Liesengang. The inset shows a close-up view of the role of a joint (marked by a dashed line) in forming iron (hydr)oxide rings. Blue bold letters and red arrows show similar geologic features in the image acquired from the UAV and the camera. The photo was taken facing west.

Sector B occupies the southeast part of the Falakra geosite with a dense concentration of cannonballs and concretions (Figures 10–12). The sector's concretions are a medley of

ovoid-like, tabular or spherical cannonballs. In addition to these, some irregularly shaped concretions also occur in all three different clusters (Figure 10).

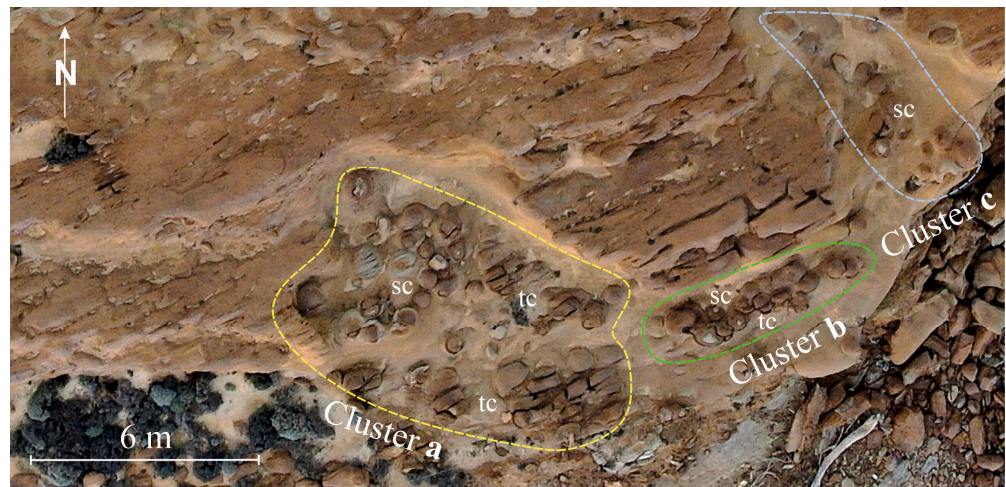


Figure 10. UAV-captured image of the sector B of the geosite, showing the geographic distribution of the three different clusters of concretions and cannonballs at the Falakra geosite.

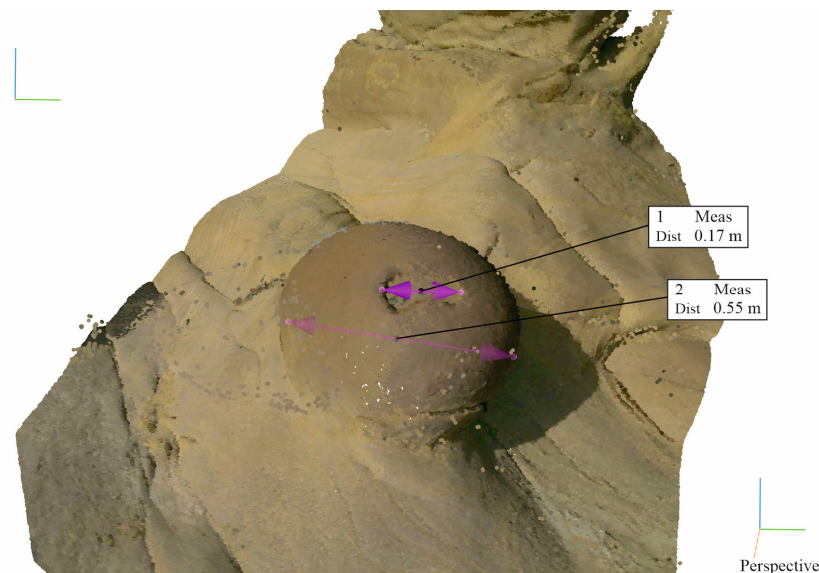


Figure 11. Three-dimensional model of a typical cannonball, displaying its diameter and the eroded portion.

The concretions in sector B range in size from 0.5 to 1.0 m in diameter. An indicative representation of a cannonball is depicted in Figure 11. The 3D model was extracted through the segmentation of the TLS point cloud. The model is fully metric, showing that the diameter of the cannonball is 0.555 m, and the eroded part is measured at 0.171 m. The erosion in each concretion or cannonball cluster varies significantly. For example, in cluster “a”, an area of 70 m², primarily spherical cannonballs and some tabular concretions are exposed. The cluster “a” area is crossed by a set of NE-trending joints (Figure 12 a and b). When the joints cross the cannonballs, they reveal a more intensive style of weathering and iron (hydr)oxide precipitation (Figure 12 a and b). Cluster “b”, covering an area of 9.5 m², comprises a dense population of primarily tabular concretions with a few spherical cannonballs (Figures 10 and 12 f). In cluster “c”, which spans an area of 20 m², the cannonballs are primarily spherical (Figures 11 and 12 e). The erosion features in this cluster are generally invariant, expressed by a small hole on top of the cannonballs (Figures 11 and 12 b, e), which is sometimes up to 0.8 m in depth (Figure 12 c and f), or by extensive spherical weathering that greatly influences the shape of the concretions (Figure 12 c). The different levels of cannonball exposure are important for sector B of the geosite; variable

levels of exposure of the cannonballs (Figures 11, 12, 13) would suggest that they rise on the surface during progressive erosion (Figure 13).

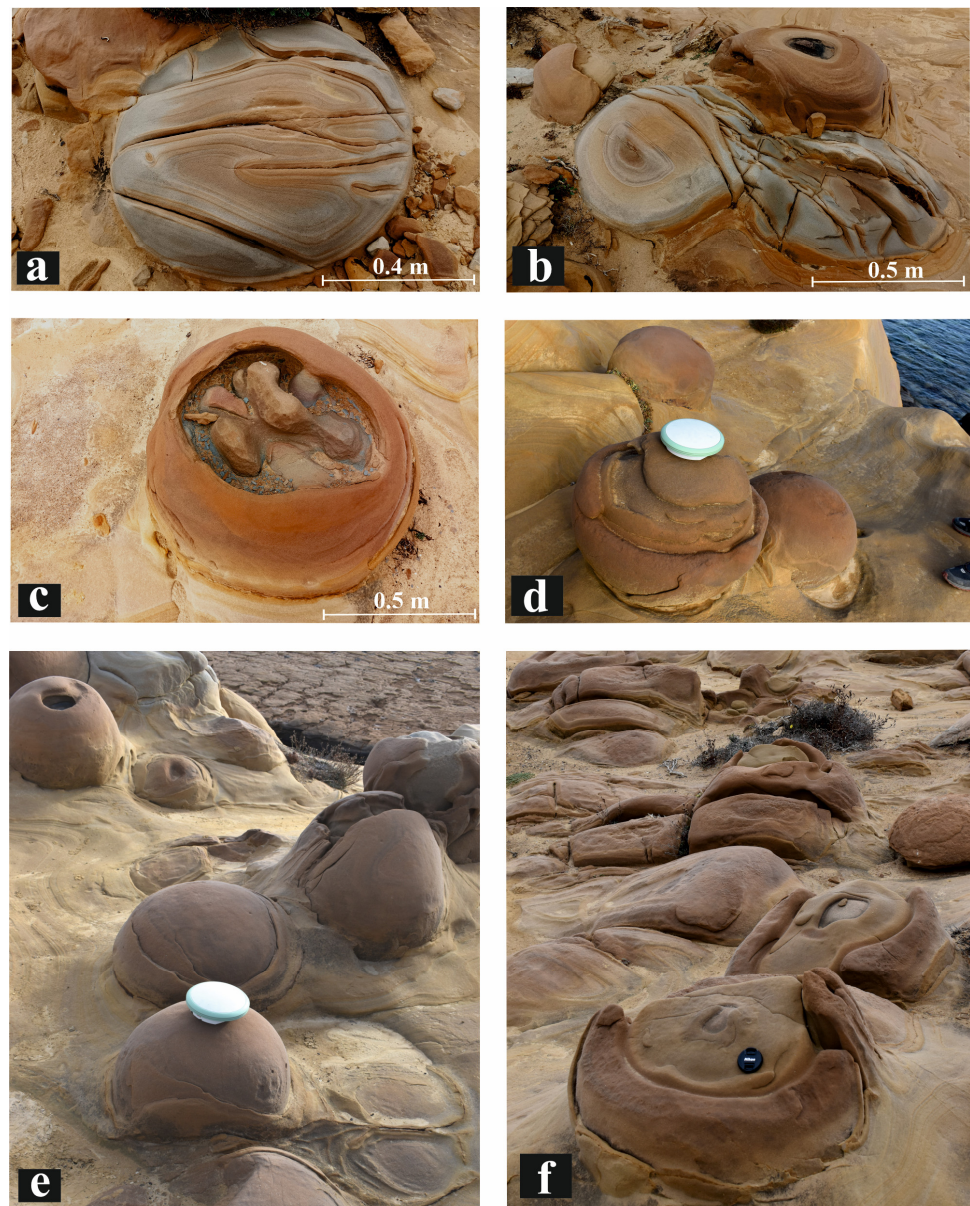


Figure 12. Various stages of evolution of cannonballs and concretions in sector B of the Falakra gessite. (a,b) The role of joints on erosion and iron oxide precipitation on an isolated complex of concretions in cluster a. For the location of cluster (a), see Figure 10. (c) Layers of sediment build-up around sandstone grits to create a cannonball. (d) Various stages of concretion protruding from the cannonballs. Note that cannonball erosion starts with the exposure of the cannonballs. These cannonballs are from cluster b in Figure 10. The GPS antenna is 19 cm in diameter and is used for scale. (e) Cannonballs jutting out, fully exposed to the landscape due to sandstone erosion. In the right corner of the photo, two cannonball casts are exposed. The GPS antenna is used for scale (19 cm in diameter). (f) Erosion rings developed in spheroidal and tabular concretions. The lens cap (6 cm in diameter) is for scale alongside the Liesegang rings.



Figure 13. (a) Cannonballs dropped from a vertical sandstone cliff, impacted by seawater and rain erosion. The photo was taken facing north, and the width of the photo represents an approximately true distance of 15 m. The box shows the location of figure (b). (b) Hard cannonballs in sandstone, as highlighted by the yellow shade, and a jutting cannonball on top of the cliff. (c) Cannonballs jutting out from the landscape due to the erosion of sandstones, alongside Liesegang rings. Liesegang rings appear to mimic the exterior of the concretions.

In summary, cannonballs or concretions undergo spheroidal weathering, exposed through rinds (Figure 12) and honeycomb erosion (see for example inset in Figure 9a). The formation of spheroidal weathered rinds is possibly related to the existence of discontinuities in rocks, which assist in the wetting of sandstone either during rain or due to the high humidity in the area (Figure 4). Similar effects may have resulted from salt spray during storms [29] rather than from frost weathering [30] (see also Figures 12 and 13). Based on our mapping and geological analysis of the three cannonballs and concretion clusters (Figure 10), we will call this sector of the geosite a “cannonball complex”.

Sector C of the geosite is characterized by the existence of joints that are correlated with the fold-related deformation in the Falakra geosite. These folds are classified as gentle and upright, with their axes trending roughly WNW. Consequently, these joints are classified according to the fold hinge trends as diagonal, longitudinal, and cross joints (Figure 14a, inset). In detail, the most well-preserved joints are classified as a pair of diagonal joints obliquely oriented to the fold axis that runs parallel to the Falakra geosite. Strike and longitudinal joints are also exposed (Figure 14a). This conjugate set of joints is best exposed on the long limb of the anticline that crosses the geosite, dipping moderately ($\approx 20^\circ$) towards ENE. In sector B, tension joints are exposed on the long limb of the anticline (Figure 10), with longitudinal and cross joints also present (Figure 14 a,b). In all these examples, the joints are accompanied by iron (hydro)oxide precipitation (Figure 14).

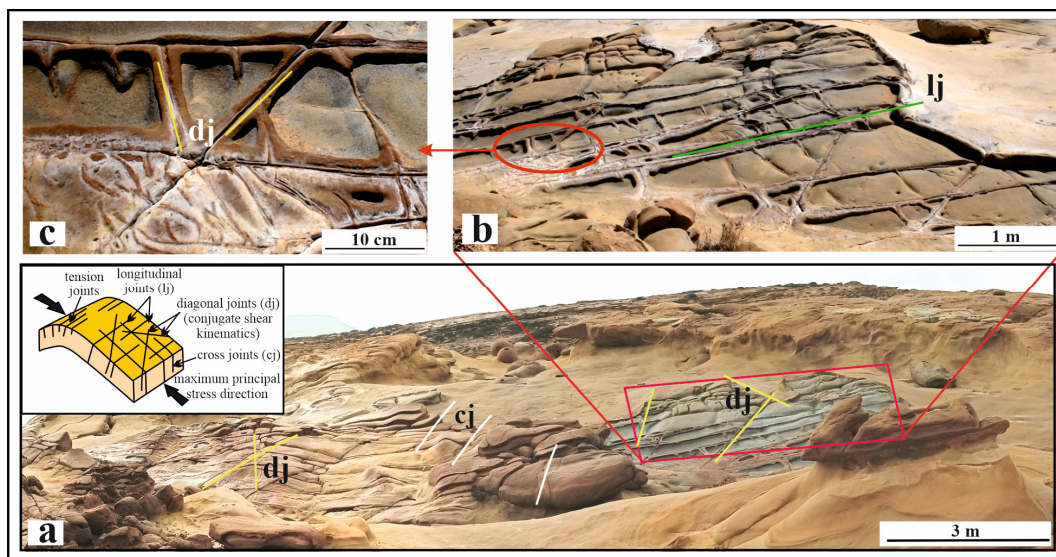


Figure 14. (a) Field photo of a fracture network from Falakra geosite, Limnos. Inset shows the classification of joints in relation to an open folding in the area. (b) Joints observed across the northeast-dipping (ca. 35°) sandstone beds from sector C in the geosite. These joints are classified as diagonal (dj) and cross joints (cj). (c) Joints bound by sandstone that are cemented by iron oxide; central cores defined by the joints appear to be iron-poor.

Sector D concentrates cannonball casts exposed in an outcrop 30 m long by 5 m wide on the bottom of a thick sandstone layer at the northern part of the geosite (Figure 15). These are essentially round to sub-round cavities, reaching up to 1.5 m in diameter, and are developed either in isolated form or in clusters (Figure 15).

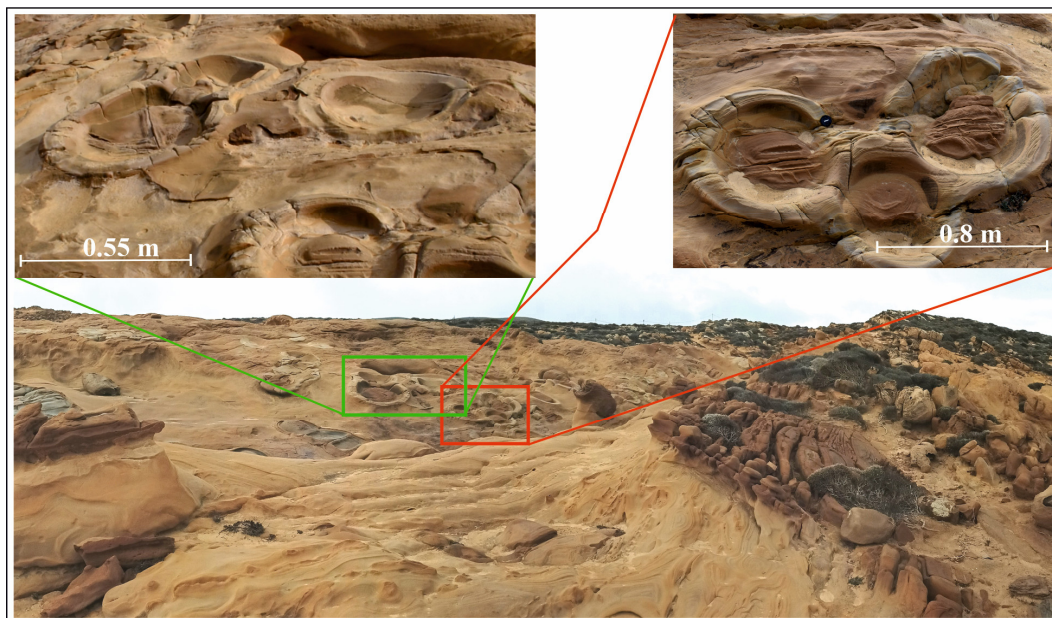


Figure 15. Relicts of eroded concretions in the geosite. Note that the casts of cannonballs in the area exhibit a similar clustering to that observed in sector B of the geosite.

The field data indicate that the casts are exposed near the base of a thick sandstone bed in the Falakra geosite. Concerning their development, we postulate that the casts probably take the shape of the lower part of a concretion or a cluster of concretions during their formation. As the cast location is close to the present-day shoreline, we consider that their dominant appearance in sector D is probably related to intensive erosion due to the sea spray effect at the rocky coastline of the Falakra geosite.

We also noted loose sand deposits throughout the geosite (Figures 6 and 15) and poor development of sand dunes beyond the west end of the Falakra geosite (Figure 7). We therefore consider that loose sand concentration (Figures 6 and 15) and dunes result from ongoing erosion at the geosite. The concentration of dunes beyond the west end of the geosite and the honeycomb structures indicate that the prevailing winds in the area (see Figure 4a) contribute to the erosion of the sandstones. These prevailing winds are strong enough to form dunes across the north coast of Limnos Island in two other localities, namely Gomati and Neftina (Figure 3). In summary, we posit that much of the cannonball outcrop and their casts in the geosite of Falakra owe their origin to the long-term exposure of the rocks to aeolian erosion.

5.3. Mineralogical and Geochemical Analysis

Mineralogical analyses reveal a simple composition for the sandstones, containing (in order of modal abundance) the minerals quartz, illite, calcite, and iron (hydr)oxides as the dominant phases. The first two represent the primary clastic components of the rocks, whereas the other two occur as abundant permeability fills. Calcite fills pore space and commonly also occurs as complex networks of veins, while iron (hydr)oxides characteristically form deposits along joints, which appear to propagate as wavy, yellowish to reddish rings within the surrounding sandstone mass. Such a distribution supports a Liesegang-style iron remobilization/re-precipitation, through the action of circulating fluids.

Geochemically, the dominance of interstitial calcite in the sandstones (>10% modal) is responsible for the atypically high concentrations of Ca relative to the PAAS standard, as displayed in the major element spidergrams of Figure 16. All other major element oxides record concentrations similar to or below those of PAAS, with Na(+Ca) and Si reflecting the dominance of clay and quartz, respectively.

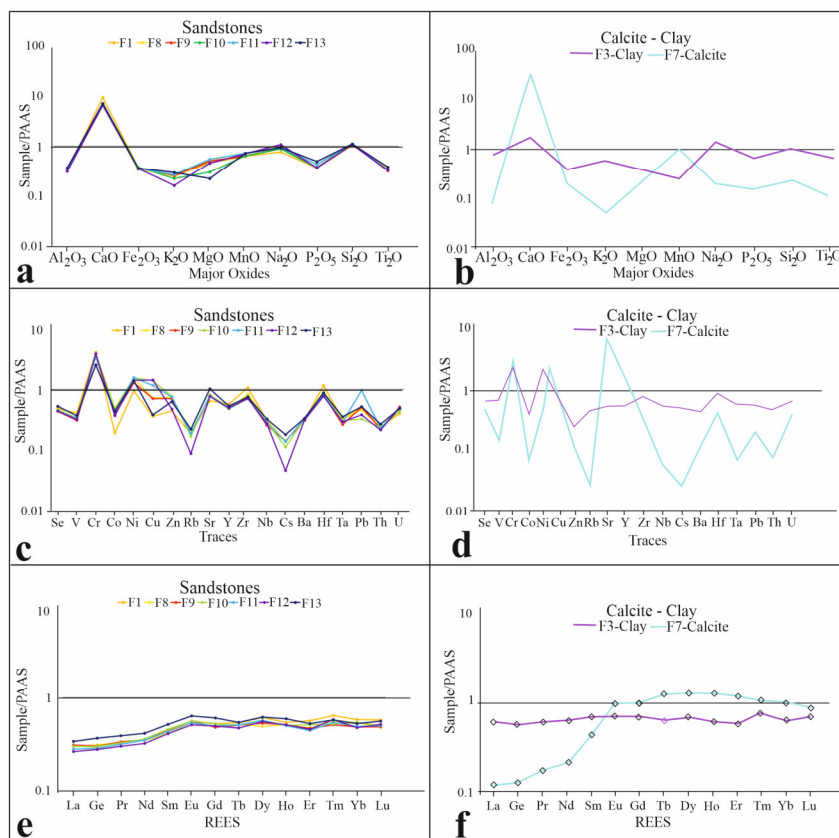


Figure 16. Major, trace, and rare-earth element (REE) spidergrams (a,c,e), respectively, for sandstone samples at Falakra, Limnos, compared to corresponding diagrams (b,d,f), respectively, for end-member calcite and illite clay samples from the same locality.

In terms of trace element abundances in the sandstones, three elements appear to record relative enrichments compared to PAAS, namely Cr, Ni, and Cu. All three of these elements can be tentatively linked to the relative contributions of calcite and clay in the sandstone samples, as illustrated in the corresponding mineral-specific spidergrams (Figure b, d, f). Further support to this interpretation is offered by the REE spidergrams of the sandstones, which reveal a consistent pattern of light REE depletion, progressively increasing values with atomic weight, followed by a flatter pattern from Eu onwards (Figure 16e). This pattern of REE behavior is mimicked—albeit in a far more pronounced manner—by the single, calcite-specific REE spidergram (Figure 16f). By contrast, the clay-dominated sample illustrates a generally flat REE pattern (Figure 16f).

6. Discussion

The sustainability assessment of geosites as tourist destinations is imperative, as these sites are considered nonrenewable resources (Ruban and Kuo 2010; Sunkar et al. 2022) [4,31]. The significance of a geosite is classified, among other factors, based on their value for science, aesthetic appeal and rarity, coupled with geosite accessibility (Wimbledon 1999; Ruban and Kuo 2010) [4,32]. Although methods and purposes of geo-conservation and the status of geosites vary greatly in different countries, irrespective of the presence or absence of relevant laws, geosites require international and local responsibility. Geosites are in most instances sensitive nonrenewable resources that require increased protection status. The maintenance of geosites is dictated largely by the monitoring of active geomorphological processes, and thus the planning of tourism for each geosite should be specified accordingly.

The current study focuses on the synergy of UAV, TLS, and GIS technologies, in conjunction with standard mineralogical and geochemical analyses, for the 3D representation and geological documentation of the Falakra geosite in Limnos. This specific geosite is strongly influenced by tourist presence and activity due to its easy accessibility (Figures 7 and 8). The proximity of the area to a dirt road increases the opportunity for sightseeing and therefore erosion due to random walking.

Modern technologies, such as UAV and TLS, are increasingly used for the 3D mapping, documentation, conservation, and promotion of geoparks and geoh heritage sites (Kyriou et al., 2024) [33]. A DJI Phantom 4 Pro quadcopter was used to map and generate 3D representations of petrified findings throughout an excavation at the Acroheiras Wind Park on Lesbos Island, Greece [34] (Papadopoulou et al., 2020). The produced DSM and orthophoto map were integrated in an augmented reality (AR) application for mobile phones. A fixed-wing UAV with a Sony camera on board was also used for the 3D stratigraphic mapping of an outcrop extended in an area of 0.52 square kilometers inside the Dinosaur Provincial Park in southeastern Alberta, Canada (Nesbit et al., 2018) [35].

Various tests assessing the effects of flight altitude and the image overlapping on the 3D representation of the Voulgaris gorge geosite in Lesbos Island were presented in another similar research study (Papadopoulou et al., 2021) [36]. The outcomes for the optimum flight altitude (80 m) of this study are in good agreement with our results. In a similar study, also based on the synergy of modern technologies along with laboratory petrological analyses (Hoblea et al., 2014) [37], field surveys were combined with classical geological mapping, GIS, and TLS to study and promote karst geoh heritage sites in Southeast France.

The Falakra formations are characterized as sandstones benches with a fine to medium grain size. These sandstone formations are believed to have been shaped by erosion. This is contrary to previous speculations that the formations are volcanic deposits and their shape is a result of the sudden contact of lavas with cold seawater, akin to volcanic pillow structures (Triantaphyllou et al., 2023)[3]. The mineralogical and geochemical results from the Falakra geosite analytical point to hydrothermal calcite being a key mineral in controlling most salient geochemical signals recorded in the sandstones. The light REE depletion in the sandstones appears to be the result of the characteristic REE pattern of calcite, with its striking mid- to heavy-REE enrichment compared to the LREE. Comparisons with the literature [38] allow for an interpretation of the origin of calcite in our case

study as having originated from hydrothermal fluid flow associated with proximal sub-volcanic activity. The relative enrichment in Cr, Ni, and Cu are likely associated with the same hydrothermal system. The more subdued geometry of the sandstone REE patterns is probably the result of the combination of the calcite REE signature with the flatter REE pattern imparted by the clay (illite) fraction of the rocks.

The above findings collectively suggest a likely low-temperature hydrothermal origin for the calcite through the ascending circulation of fluids equilibrating with basic to intermediate volcanic rocks in the broader region. In the absence of stable isotope data, we are unable to provide any constraints on the exact origin and temperature of the fluids. We are inclined, however, to draw parallels with similar evidence of low-temperature, volcanic-driven hydrothermal fluid-flow and carbonate deposition shaping a geomorphologically analogous locality of sandstone formations in Scotland [39].

Since the shape and exposure of the Falakra formations are primarily influenced by aeolian erosion and the wetting of sandstones, it is crucial to calculate the mean annual erosion rates in order to constrain their evolution in the near future and their sustainability as geoheritage monument. For a site under continuous touristic stress such as the Falakra geosite, knowledge of the erosion process is particularly crucial. In this light, some previous studies have attempted to estimate the erosion rate on sandstone shore formations in South-eastern Australia (Yuan et al., 2020) [40] and on an experimental assembly in the countryside of Belfast in Northern Ireland (McAllister et al., 2017)[41].

The analysis of the meteorological data provided an overview of the parameters acting on the erosion processes of the geosite. In a next stage of the research, systematic mapping of such processes will be implemented through repeated laser scanning surveys of the geosite to identify the erosion rate. These measurements will be combined with the installation of a meteorological station at the observation site to evaluate how meteorological parameters affect the geosite.

Each geosite is a sensitive, nonrenewable resource characterized by its own set of physiological parameters and anthropogenic influences. These will dictate in each instance the maintenance strategy of the site, monitoring of active geomorphological processes, and planning of tourist access and activity. With specific reference to Falakra, the site is exposed to complex, continuous erosional processes in a coastal environment. These render Falakra as an environmentally fragile geosite.

Current practices for the protection of the geosite only impose restrictions on the removal of resources. Our work indicates that the range of restrictions at the geosite must be expanded. New restrictions are to be established and communicated through clear signposting. Indicative labels should include: *“Please leave flowers, stones, and other natural objects where you found them. Preserve the privilege for other visitors to enjoy the unique Falakra geosite. It is illegal to walk freely through the geosite. Free access to the geosite increases erosional damage; work with us to maintain the site for future visitors”*.

The second key step will be constructing a network of trails through the geosite, along with regular platforms for the visitors to stop at important stations to engage with and appreciate the evolution of the geosite (Figure 17). Given the location of the geosite near the seafront, we propose that these trails be constructed with serrated steel grating.

The proposed trails in Figure (17) are trying to enhance the visitor experience by offering safe, enjoyable routes that showcase the beauty of the geologically discrete sectors in the Falakra geosite. In addition, these trails ensure the increased protection of the geological and geomorphological features because they will minimize the tourists' free access to the geosite. The pre-defined route will reduce human-induced erosion or removal of rocks during tourists' walk through the geosite, in contrast to the current practice of free walking through the geosite. Furthermore, a safe trail will increase tourist footfall and maybe small businesses. These trails will extend the geosite's accessibility to a broader audience, such as families with young children and older adults.

However, it should be noted that the best practices for the conservation of a geosite is not a simple task and needs further research and collection of new data. Thus the definition of the best practices for the conservation of Falakra geosite is out of the scope of this study.



Figure 17. Orthophoto map overlapped with a hill-shaded DSM of Falakra geosite. The map shows the sectors of significance and suggested paths through the geosite and selected locations of platforms, orange boxes, with their elevations. Platform (a) is for unobstructed observation of the lander-like landscape, platform (b) is for viewing clusters of concretions and cannonballs, and platform (c) is for observation of eroded concretions and joints accompanied by iron (hydro)oxide precipitation. The continuous blue line shows the 380 m long round-trip path through the geosite, which helps visitors to see all geological formations of aesthetic value. The dashed blue line indicates an additional path and the platform (d) for the unobstructed observation of the entire geosite.

7. Conclusions

The Falakra geosite is a unique geoheritage monument under touristic pressure that needs a well-documented protection plan and sustainable development and conservation. The geosite is significant for understanding the geological evolution of the area, it is of high aesthetic value, and includes rare formations within a local and international context. Since the geosite receives little structured protection, we propose a series of actions towards a sustainable conservation plan.

1. Detailed 3D mapping of the geosite using modern remote sensing technologies such as UAV and TLS provides significant steps towards the protection planning of the geosite.
2. The Falakra geosite includes cannonball concretions, joints with iron (hydr)oxide precipitates, honeycomb erosion features, Liesegang rings, and cannonball casts. All these are geological marvels and invaluable tools for unravelling the recent geological history of northern Limnos. The cannonball casts, in particular, are a rarely preserved feature documented for the first time in the Falakra geosite.
3. Contrary to previous geological interpretations for the strong influence of volcanic activity on the formation of the Falakra geosite, we provide evidence that the geosite is the combined result of aggressive coastal sandstone erosion that exposing a series of spectacular landforms. The latter would have formed under the influence of a low-temperature, volcanic-driven hydrothermal fluid–rock interaction system, accompanied by widespread carbonate deposition, as in the case of similar sites in Scotland [39].

4. Easy access to the geosite through nearby roads, combined with the low relief and mild climatic conditions in the area, attracts a significant number of tourists that impart a strong anthropogenic footprint. In view of the naturally fragile environment at the geosite, the elimination of excessive human–site interaction is imperative for effective site conservation.
5. To further enhance the protection of the geosite, we propose annual 3D monitoring to estimate the mean annual erosion rate and likelihood of damage in light of public access.
6. As first action for the protection of the geosite, we propose the construction of sign-posted trails and platforms at the site. These trails will raise awareness of geosite protection and increase the safety of visitors. To fulfil these conditions, the trails must be constructed with serrated steel grating.

Supplementary Materials: we noticed that supplementary materials was not cited in the main text. Please add the missing citation and check the main text carefully.

Author Contributions: Conceptualization, I.K.K. and K.G.N.; methodology, I.K.K. and A.K.; investigation, I.K.K., K.G.N., H.T., and G.D.; resources, I.K.K.; data curation, I.K.K., K.G.N., H.T., and G.D.; writing—original draft preparation, I.K.K., A.K., K.G.N., I.P., and H.T.; visualization, A.K. and I.P.; supervision, I.K.K.; project administration, I.K.K.; funding acquisition, I.K.K. All authors have read and agreed to the published version of the manuscript.

Funding: “This research was partially funded by the Municipality of Lemnos”

Data Availability Statement: The data presented in this study are available on request from the corresponding author due to the on-going research.

Acknowledgments: In this section, you can acknowledge any support given which is not covered by the author contribution or funding sections. This may include administrative and technical support, or donations in kind (e.g., materials used for experiments).

Conflicts of Interest: George Dimaris is self employee in George Dimaris Technical Office. The authors declare no conflicts of interest.

References

1. Statistical Bulletin no 90. Available online: https://insete.gr/wp-content/uploads/2024/04/Bulletin_EN_2023.pdf (accessed on 15 May 2024).
2. Enterprise Greece. Available online: <https://www.enterprisegreece.gov.gr/newsletters/newsletter-articles/greece-visitor-arrivals-jump-tourism-data-points-to-record-setting-year-ahead/> (accessed on 10 December 2024).
3. Triantaphyllou, M.V.; Firkasis, N.; Tsourou, T.; Vassilakis, E.; Spyrou, E.; Koukousioura, O.; Oikonomou, A.; Skentos, A. “Geo-Archaeo-Routes” on the Island of Lemnos: The “Nalture” Experience as a Holistic Geotouristic Approach within the Geoethical Perspective. *Geosciences* **2023**, *13*, 143. <https://doi.org/10.3390/geosciences13050143>.
4. Kokkalas, S.; Xypolias, P.; Koukouvelas, I.K.; Doutsos, T. Post-Collisional Contractional and Extensional Deformation in the Aegean Region. In *Post-Collisional Tectonics and Magmatism in the Mediterranean Region and Asia*; Dilek, Y., Pavlides, S., Eds.; Geological Society of America Special Paper: Washington, DC, USA, 2006; Volume 409, pp. 97–123.
5. Global Geoparks Network. Available online: <http://www.globalgeopark.org/GeoparkMap/geoparks/Greece/index.htm> (accessed on 1 December 2024).
6. Herrera-Franco, G.; Carrión-Mero, P.; Montalván-Burbano, N.; Caicedo-Potosí, J.; Berrezueta, E. Geoheritage and Geosites: A Bibliometric Analysis and Literature Review. *Geosciences* **2022**, *12*, 169. <https://doi.org/10.3390/geosciences12040169>.
7. García-Ortiz, E.; Fuertes-Gutiérrez, I.; Fernández-Martínez, E. Concepts and terminology for the risk of degradation of geological heritage sites: Fragility and natural vulnerability, a case study. *Proc. Geol. Assoc.* **2014**, *125*, 463–479. <https://doi.org/10.1016/j.pgeola.2014.06.003>.
8. Macario Barros, A.; Michel, M.; Moline, Y.; Corre, G.; Carrel, F. A Comprehensive Survey of Visual SLAM Algorithms. *Robotics* **2022**, *11*, 24. <https://doi.org/10.3390/robotics11010024>.
9. Westoby, M.; Brasington, J.; Glasser, N.; Hambrey, M.; Reynolds, J. Structure-from-Motion’ photogrammetry: A low-cost, effective tool for geoscience applications, *Geomorphology* **2012**, *179*, 300–314.

10. Micheletti, N.; Chandler, J.; Lane, S.N.; Chapter 2—Structure from motion (SFM) photogrammetry., In *Geomorphological Techniques*; Section 2.2; British Society for Geomorphology: London, UK, 2015.
11. Smith, M.W.; Carrivick, J.L.; Quincey, D.J. Structure from motion photogrammetry in physical geography. *Prog. Phys. Geogr. : Earth Environ.* **2016**, *40*, 247–275.
12. Kyriou, A.; Nikolakopoulos, K.; Koukouvelas, I. How Image Acquisition Geometry of UAV Campaigns Affects the Derived Products and Their Accuracy in Areas with Complex Geomorphology. *ISPRS Int. J. Geo-Inf.* **2021**, *10*, 408.
13. Nikolakopoulos, K.G.; Kyriou, A.; Koukouvelas, I.K. Developing a Guideline of Unmanned Aerial Vehicle's Acquisition Geometry for Landslide Mapping and Monitoring. *Appl. Sci.* **2022**, *12*, 4598.
14. Koukouvelas, I.; Doutsos, T. Tectonic stages along a traverse cross cutting the Rhodopian zone (Greece), *Geol. Rundsch.* **1990**, *79*, 753–776.
15. Roussos, N. Geological Map of Greece 1/50.000 Moudros and Myrina Sheet, Editions; Institute of Geology and Mineral Exploration: Athens, Greece.
16. Innocenti, F.; Manetti, P.; Mazzuoli, R.; Pertusati, P.; Fytikas, M.; Kolios, N.; Vougioukalakis, G.E.; Androulakakis, N.; Critelli, S.; Caracciolo, L. Geological Map (Scale 1:50,000) of Limnos Island (Greece): Explanatory notes. *Acta Vulcanol.* **2009**, *21*, 123–134.
17. Mavromatidis, V.C.; Kelessidis, K.; Monopolis, D. A review of recent hydrocarbon exploration in Greece and its potential. In Proceedings of the 1st International Conference AMIREG, Chania, Greece, 7–9 June 2004.
18. Maravelis, A.; Konstantopoulos, P.; Pantopoulos, G.; Zelilidis, A. North Aegean sedimentary basin evolution during Late Eocene to Early Oligocene time: Based on the sedimentological studies at the Lernnos Island, NE Greece. *Geol. Carpathica* **2006**, *58*, 455.
19. Okay, A.I.; Özcan, E.; Siyako, M.; Bürkan, K.A.; Kylander-Clark, A.R.C.; Bidgood, M.D.; Shaw, D.; Simmons, M.D. Thrace basin—An Oligocene clastic basin formed during the exhumation of the Rhodope Complex. *Tectonics* **2023**, *42*, e2023TC007766. <https://doi.org/10.1029/2023TC007766>.
20. Maravelis, A.; Boutelier, D.; Catuneanu, O.; Seymour, K.S. A review of tectonics and sedimentation in a forearc setting: Hellenic Thrace Basin, North Aegean Sea and Northern Greece. *Tectonophysics* **2016**, *674*, 1–19.
21. Innocenti, F.; Manetti, P.; Mazzuoli, R.; Pertusati, P.; Fytikas, M.; Kolios, N. The geology and geodynamic significance of the Island of Limnos, North Aegean Sea, Greece, *Neues Jahrb. Geol. Palaeontol. Monatsh.* **1994**, *1994*, 661–691.
22. Pe-Piper, G.; Piper, D.J.; Koukouvelas, I.; Dolansky, L.M.; Kokkalas, S. Postorogenic shoshonitic rocks and their origin by melting underplated basalts: The Miocene of Limnos, Greece. *Geol. Soc. Am. Bull.* **2009**, *121*, 39–54. <https://doi.org/10.1130/B26317.1>.
23. Koukouvelas, I.K.; Pe-Piper, G.; Piper, D.J.W.; Kokkalas, S.; Dolansky, L.M. The Miocene volcanism of Limnos, NE Greece. In Proceedings of the Scientific meeting Geological Society of Greece «Geology of Thrace and Seismotectonics of NE Aegean» Samothraki, Aegean Sea, 2–4 September 2005; pp. 53–54.
24. Koukouvelas, I.K.; Aydin, A. Fault Structure and Related Basins of the North Aegean Sea and Its Surroundings. *Tectonics* **2002**, *21*, 1–17.
25. Tranos, M.D. Faulting of Lemnos Island; a mirror of faulting of the North Aegean Trough (Northern Greece). *Tectonophysics* **2009**, *467*, 72–88. <https://doi.org/10.1016/j.tecto.2008.12.018>.
26. Hellenic National Meteorological Service. Available online: http://emy.gr/emy/el/climatology/climatology_city?perifereia=North%20Aegean&poli=Lemnos (accessed on 1 December 2024).
27. Cvancara, A.M. Technical Report: Geology of the Cannonball Formation (Paleocene) in the Williston basin, with reference to uranium potential. Report of investigation No. 57, U.S. Department of Energy, Office of Scientific and Technical Information, 1976, 32, <https://www.osti.gov/biblio/7341755>.
28. Jackson, J.A. *Glossary of Geology*, 4th ed.; American Geological Institute, Alexandria, VA, USA, 1997; p. 366.
29. Smith, B.J.; Warke, P.A.; McGreevy, J.P.; Kane, H.L. Salt-weathering simulations under hot desert conditions: Agents of enlightenment or perpetuators of preconceptions?, *Geomorphology* **2005**, *67*, 211–227.
30. Williams, R.B.G.; Robinson, D.A. Weathering of sandstone by the combined action of frost and salt. *Earth Surf. Process. Landforms* **1981**, *6*, 1–9.
31. Sunkar, A.; Laksapriyanti, A.P.; Haryono, E.; Brahmi, M.; Setiawan, P.; Jaya, A.F. Geotourism Hazards and Carrying Capacity in Geosites of Sangkulirang- Mangkalihat Karst, Indonesia. *Sustainability* **2022**, *14*, 1704. <https://doi.org/10.3390/su14031704>.
32. Wimbledon, W. GEOSITES—A new conservation initiative. *Episodes* **1999**, *19*, 87–88.
33. Kyriou, A.; Nikolakopoulos, K.; Papadopoulou, P.; Tzortzi, M.; Golfinopoulos, V.; Tsoni, M.; Iliopoulos, G. 3d mapping of geological heritage: The case of the mythical waterfall of Styx. In *Earth Resources and Environmental Remote Sensing/GIS Applications XV*; Proc. SPIE: Washington, DC, USA, 2024; Volume 13197, p. 1319713.

34. Papadopoulou, E.-E.; Kasapakis, V.; Vasilakos, C.; Papakonstantinou, A.; Zouros, N.; Chroni, A.; Soulakellis, N. Geovisualization of the Excavation Process in the Lesvos Petrified Forest, Greece Using Augmented Reality. *ISPRS Int. J. Geo-Inf.* **2020**, *9*, 374. <https://doi.org/10.3390/ijgi9060374>.
35. Nesbit, P.R.; Durkin, P.R.; Hugenholtz, C.H.; Hubbard, S.H.; Kucharczyk, M. 3-D stratigraphic mapping using a digital outcrop model derived from UAV images and structure-from-motion photogrammetry: *Geosphere* **2018**, *14*, 2469–2486. <https://doi.org/10.1130/GES01688.1>.
36. Papadopoulou, E.-E.; Papakonstantinou, A.; Zouros, N.; Soulakellis, N. Scale-Variant Flight Planning for the Creation of 3D Geovisualization and Augmented Reality Maps of Geosites: The Case of Voulgaris Gorge, Lesvos, Greece. *Appl. Sci.* **2021**, *11*, 10733. <https://doi.org/10.3390/app112210733>.
37. Hoblea, F.; Delannoy, J.J.; Jaillet, S.; Ployon, E.; Sadier, B. Digital Tools for Managing and Promoting Karst Geosites in Southeast France, *Geoheritage* **2014**, *6*, 113–127. <https://doi.org/10.1007/s12371-014-0112-1>.
38. Debruyne, D.; Hulsbosch, N.; Muchezet, P. Unraveling Rare Earth Element Signatures in Hydrothermal Carbonate Minerals Using a Source–Sink System." *Ore Geol. Rev.* **2016**, *72*, 232–252. <https://doi.org/10.1016/j.oregeorev.2015.07.022>.
39. Hudson, J.D.; Paxton, R.B.; Andrews, J.E.; Dennis, P.F.; Marca, A.D. Classic Scottish sandstone concretions formed from hot water. *Geol. Today* **2023**, *39*, 231–235.
40. Yuan, R.; Kennedy, D.M.; Stephenson, W.J.; Finlayson, B.L. The multidecadal spatial pattern of erosion on sandstone shore platforms in south-eastern Australia, *Geomorphology* **2020**, *371*, 107437. <https://doi.org/10.1016/j.geomorph.2020.107437>.
41. McAllister, D.; Warke, P.; McCabe, S., Stone temperature and moisture variability under temperate environmental conditions: Implications for sandstone weathering, *Geomorphology* **2017**, *280*, 137–152. <https://doi.org/10.1016/j.geomorph.2016.12.010>.

Disclaimer/Publisher’s Note: The statements, opinions and data contained in all publications are solely those of the individual author(s) and contributor(s) and not of MDPI and/or the editor(s). MDPI and/or the editor(s) disclaim responsibility for any injury to people or property resulting from any ideas, methods, instructions or products referred to in the content.